# Structural and Vibrational Properties of Tetraoxaporphyrin Dication, the Oxygen Analogue of Porphyrin, and of Isoelectronic Diprotonated Porphyrin

**Ivana Jelovica,[†] Laura Moroni, Cristina Gellini, and Pier Remigio Salvi***

*Dipartimento di Chimica, Universitá di Firenze, via della Lastruccia 3, 50019 Sesto Fiorentino, Firenze, Italy*

**Nada Orlić**

*Faculty of Philosophy, Physics Department, University of Rijeka, Omladinska 14, Rijeka, Croatia*

*Received: May 31, 2005; In Final Form: September 13, 2005*

Structural calculations by means of the density functional method have been performed on tetraoxaporphyrin dication and on isoelectronic diprotonated porphyrin as well as on the sulfur and carbon analogues of porphyrin. A detailed study of the stable conformations of these compounds is reported starting with the most symmetrical conformations and lowering the symmetry along the vibrational coordinates with imaginary frequency. The calculated geometries are related to experimental structures available from X-ray diffraction studies. The Raman spectra of tetraoxaporphyrin dication exciting with micro-Raman instrumentation at 785 nm and of diprotonated porphyrin in near-resonance conditions with the Soret band have been measured. The correlation between frequencies calculated with the DF/B3-LYP/cc-pVDZ procedure for porphyrin, diprotonated porphyrin, and tetraoxaporphyrin dication has allowed for making a vibrational assignment for the latter two systems in excellent agreement with experiment using a single frequency scale factor.

## I. Introduction

Porphyrins, constituting pyrrolic macrocycles, have attracted interdisciplinary interest since their molecular design and multiple functions allow applications in many fields of science.[1] Referred to as the pigments of life,[2] these macrocycles play an important role in diverse biological processes. Thus chlorophyll, causing light absorption in green plants, is the pigment responsible for photosynthesis, whereas heme, the pigment of blood, functions as oxygen transport and storage in aerobic organisms. In addition, porphyrins serve as essential components in technical devices of various kinds and hence have become an integral part in material science.[3,4] As a prominent example of medicinal applications of porphyrins their property to act as a sensitizer in photodynamic therapy must be cited.[5]

As a fundamental ring system, porphyrin (**2**), in Figure 1, has been the subject of intense spectroscopic and structural investigations.[6] These studies, in conjunction with the thermodynamic stability of porphyrin, attest to the aromatic character of the molecule. In accord herewith, the electronic structure of (**2**) has been frequently discussed in terms of conjugation pathways with $(4n + 2)$ $\pi$ electrons in substructures embedded into the macrocycle and constrained to planarity by the insertion of inner and/or outer bridges.[7,8] Despite the intrinsic plausibility of this approach, simple Hartree−Fock results predict single/double bond alternation along the periphery of the system, in contrast with the experimental observation. It is necessary to include the electron correlation into the computational procedure to match observed bond-equalized geometries. For instance, a stable geometry of $D_{2h}$ symmetry, as indicated by the X-ray diffraction data,[9] was obtained for porphyrin either considering the MP2 perturbative correction to the HF energies or using the density functional (DF) treatment.[10,11] Further, molecules such as the diprotonated species and the oxygen and sulfur dicationic analogues, (**3**), (**4**), and (**5**) in Figure 1, respectively, have structures determined not only by the cyclic $\pi$-electron overlap but, as far as (**3**) and (**5**) are concerned, also by the steric interaction between the four central hydrogen atoms, as to (**3**), and the four heteroatoms, as to (**5**). In fact, while (**4**) is a square planar macrocycle,[12] (**5**) has a puckered conformation in the crystal,[13] and diprotonated porphyrins have structures more or less distorted from planarity depending upon the peripheral substitution.[14−16] Nonplanar porphyrin-type molecules may have more than one energy minimum, as it has been shown for (**3**), for which two stable conformations, the first (and lowest) with $D_{2d}$ and the second with $C_i$ symmetry, have been reported.[17] This point invites for a parallel study on (**5**).

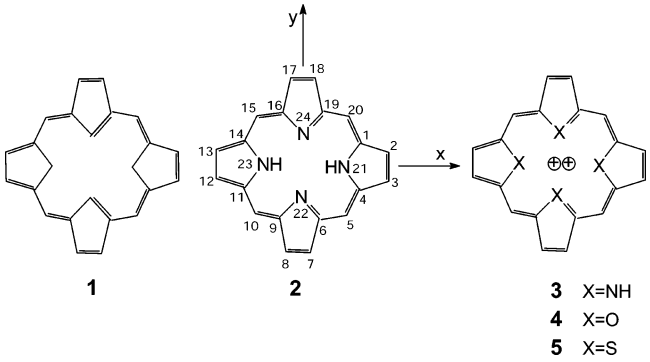


**Figure 1.** The molecular structures of porphyrin (**2**), the carbon analogue of porphyrin (**1**), diprotonated porphyrin (**3**), tetraoxaporphyrin (**4**), and tetrathiaporphyrin (**5**) dications. The atomic numbering of the carbon and hetero (N, O, S) atoms and the molecular reference system are common to all the structures and shown for convenience only for (**2**). Atoms 1, 4, 6, 9, 11, 14, 16, and 19 are denoted as α, atoms 2, 3, 7, 8, 12, 13, 17, and 18 as $\beta$, and atoms 5, 10, 15, and 20 as *meso*.

* To whom correspondence should be addressed. E-mail: piero.salvi@unifi.it.

[†] On leave from the Faculty of Philosophy, Physics Department, University of Rijeka, Croatia.

10.1021/jp052872z CCC: $30.25 
Published on Web 10/19/2005

Therefore, in the first part of this study the structural properties of (**3**)−(**5**) are investigated by means of the DF method. For the sake of completeness, the computational analysis has been extended also to the as yet unknown carbon analogue of porphyrin (**1**), in Figure 1. The search for extrema over the ground-state energy surface of (**1**)−(**5**) requires a surface scan with the highest accuracy possible. In the last years our group has reported on the structural properties of bridged [10]- and [14]annulenes relying on the DF computational technique and using the B3-LYP exchange-correlation functional and highly correlated basis functions such as the cc-pVDZ set.[18,19] Calculated geometries were found in excellent agreement with experiment.[18,19] It is reasonable to think that the DF/B3-LYP/cc-pVDZ combination is equally adequate to deal with the subtle conformational changes occurring in the (**1**)−(**5**) series.

The second part of the paper starts with the consideration that the shape of the energy surfaces around the minima is related to the vibrational properties of the porphyrin-type macrocycle both in terms of frequencies and of infrared and Raman intensities. Ultimately, we wish to provide a high quality force field for (**3**) and (**4**) and by means of it a well-founded vibrational assignment. DF methods are suited for this purpose, as it has been shown in several papers.[18−22] Experimentally, we have measured the Raman spectra of (**3**) and (**4**), molecules available to our group and not yet investigated with this technique. In contrast with the scarcity of vibrational data on (**3**) and (**4**) a large set of data is available on (**2**). Nonresonant and resonant Raman results on porphyrin[23,24] as well as infrared, fluorescence, and phosphorescence data on porphyrin in rare gas matrices[25−27] have allowed to propose an accurate force field derived from DF/B3-LYP/6-31G* calculations and scaled according to appropriate factors.[23,28] On the basis of our DF/B3-LYP/cc-pVDZ results a vibrational assignment of (**2**) has been achieved completely consistent with that reported[23,28] and using a single frequency scale factor. This gives weight also to the proposed vibrational assignment regarding (**3**) and (**4**).

## II. Experimental Section

The perchlorate salt of tetraoxaporphyrin dication (**4**), prepared following the reported synthetic route,[12] was a generous gift from Prof. E. Vogel (University of Köln, Germany). Porphyrin (**2**) from Frontier Scientific (U.S.A.) was used as received.

Two independent instrumentations were used for the Raman experiments. The first is a micro-Raman apparatus (Renishaw RM 2000) equipped with a microscope objective, two notch holographic filters, and a single grating monochromator and coupled to two external low-power laser sources, i.e., a diode laser emitting in the near-infrared (785 nm) and an argon laser emitting in the green region of the visible (514 nm). The sample was a tiny crystal of (**4**). Since (**4**) absorbs in the visible,[12] the Raman spectrum was acquired with near-infrared excitation. Also, the irradiation was kept at low power values, ≤4 mW, to avoid any thermal damage of the crystal. The backscattered radiation, collected, filtered, and dispersed through the optical system, was gathered onto a charge-coupled device (CCD, Renishaw) cooled to ≈ −70 °C. Different points of the tiny crystal were probed with the laser excitation, and the scattered radiation was collected for a time ranging from a few seconds to ≈1 min. The spectrum does not change appreciably, regardless of the incidence point and of the collection time. Looking after the experiment at the irradiated sample through the microscope objective, no damage was seen on the surface.

Solutions of (**2**) in benzene, $c \approx 7 \cdot 10^{-4}$ M, were freshly prepared for the second series of Raman experiments. As to (**3**), the species was obtained in acid solution at very low pH, as it results from the comparison of our spectrum in the visible region with that of a recent report.[17] Solutions of (**3**) in HCl and $HClO_4$, $c \approx 3 \times 10^{-4}$ M, and of (**2**) were excited at room temperature with the 406.7 and the 413.1 nm lines of a $Kr^+$ laser, on the edge of the strong Soret band. The laser power was ≈15 mW, low enough not to induce undesired thermal effects. The Raman spectra in near-resonance with the Soret band were obtained either with standard collection/detection instrumentation (computer-controlled double Jobin-Yvon monochromator, ≈6 $cm^{-1}$ spectral resolution; red-extended cooled photomultipler; photon counting apparatus) or with a triple spectrometer (Acton Research) coupled to a liquid nitrogen-cooled CCD detector (Princeton Instruments). The results being identical while the acquisition time in the second case much shorter than in the first, it turns out that under our experimental conditions no thermal deterioration occurs in the solutions even after relatively prolonged irradiation. As a last check, the UV/vis absorption spectra after each Raman experiment did not signal spectral changes with respect to the initial spectra.

## III. Ground-State Energy Extrema

All ab initio calculations were performed with the Gaussian program package,[29] using the B3-LYP exchange-correlation functional and the cc-pVDZ basis set. As already noted in the Introduction, the combination of the DF method with accurate basis sets improves considerably the quality of structural and vibrational calculations.[18−22] Our structural results are collected in Table 1.

We have identified minima and maxima on the ground-state energy surface of the molecules drawn in Figure 1 with the following procedure. First, the structure was optimized within a given point group symmetry starting with the highest symmetry which is compatible with the system under consideration. This is $D_{2h}$ for (**1**) and (**2**) and $D_{4h}$ for all the others, (**3**)−(**5**). The optimized geometry is a stable energy minimum when all the calculated vibrational frequencies are real. On the contrary, the occurrence of imaginary frequencies indicates that the structure lies on an energy maximum with respect to the corresponding coordinates. Displacing the molecules along these coordinates the geometry optimization and the vibrational calculation is repeated until no imaginary frequency is found. Following this procedure a number of extrema, i.e., minima and maxima, have been located on the ground-state energy surface.

Starting with the $D_{2h}$ structure of (**1**), CC bonds 1−2, 2−3, 4−5, 5−6, and 6−22 (see Figure 1 for atomic numbering) have approximately constant length, ≈1.410 Å, while the 1−21 bond is single, 1.503 Å, and 7−8 almost double, 1.361 Å. These data substantiate the view that (**1**) includes a delocalized substructure with 18 C atoms, i.e., the cycle connecting the C atoms 1, 2, ..., 6, 22, 9, 10, 11, 12, ..., 16, 24, 19, 20. The $D_{2h}$ structure is not a minimum on the ground-state surface, since one $b_{1u}$ normal mode has an imaginary frequency, $29i$ $cm^{-1}$. Lowering the symmetry along this mode a nonplanar $C_{2v}$ minimum, with energy only ≈0.1 kcal/mol lower, is obtained. Apart from the very weak nonplanarity of the $C_{2v}$ geometry, the two calculated structures are almost identical. Given the small energy difference, this might indicate that the present calculation underestimates slightly the electron correlation in (**1**).

As far as (**2**) is concerned, we first recall that porphyrin has been studied extensively with ab initio methods.[10,11,30−32] It has been generally found that including electron correlation high-symmetry structures become considerably lower in energy than the corresponding structures with reduced symmetry. In par-

**TABLE 1: Calculated(DF/B3-LYP/cc-pVDZ) and Experimental Bond Lengths (Å) of the Stable Structures of (1)−(5)[e]**

| | | | | (3) | | | | | | (5) | | | |
|---|---|---|---|---|---|---|---|---|---|---|---|---|---|
| | | (2) $D_{2h}$ | | $D_{2d}$ | | | | (4) $D_{4h}$ | | | $C_{2h}$ | | |
| | (1) $C_{2v}$ | calc | exp[a] | calc | exp[b] | $C_i$ | $C_1$ | calc | exp[c] | $C_{4v}$ | calc | exp[d] | $C_{2v}$ |
| 1−2 | 1.415 | 1.437 | 1.430 | 1.431 | 1.422/1.431 | 1.438 | 1.437 | 1.421 | 1.405 | 1.431 | 1.428 | 1.412 | 1.432 |
| 2−3 | 1.406 | 1.375 | 1.365 | 1.378 | 1.354/1.366 | 1.375 | 1.375 | 1.377 | 1.341 | 1.384 | 1.387 | 1.363 | 1.383 |
| 3−4 | | | | | | 1.436 | 1.438 | | | | | | |
| 4−5 | 1.403 | 1.396 | 1.387 | 1.399 | 1.400/1.414 | 1.400 | 1.400 | 1.391 | 1.375 | 1.411 | 1.415 | 1.405 | 1.411 |
| 5−6 | 1.413 | 1.402 | 1.376 | | | 1.398 | 1.399 | | | | 1.411 | 1.392 | 1.411 |
| 6−7 | 1.482 | 1.462 | 1.452 | | | 1.425 | 1.426 | | | | 1.431 | 1.429 | 1.431 |
| 7−8 | 1.361 | 1.359 | 1.345 | | | 1.381 | 1.381 | | | | 1.387 | 1.355 | 1.385 |
| 8−9 | | | | | | 1.427 | 1.425 | | | | | | |
| 9−10 | | | | | | 1.399 | 1.398 | | | | | | |
| 10−11 | | | | | | 1.400 | 1.400 | | | | | | |
| 1−21 | 1.504 | 1.372 | 1.380 | 1.395 | 1.371/1.390 | 1.381 | 1.381 | 1.366 | 1.367 | 1.753 | 1.756 | 1.727 | 1.754 |
| 4−21 | | | | | | 1.382 | 1.380 | | | | | | |
| 6−22 | 1.412 | 1.365 | 1.376 | | | 1.408 | 1.406 | | | | | | |
| 9−22 | | | | | | 1.405 | 1.409 | | | | 1.753 | 1.721 | 1.753 |

[a] From ref 9, average values of distances symmetrically equivalent in $D_{2h}$ symmetry. [b] From ref 16, average values of distances symmetrically equivalent in $D_{2d}$ symmetry for $(H_4TMP)^{2+}$, first entries, and $(H_4TPP)^{2+}$, second entries. [c] From ref 12, average values of distances symmetrically equivalent in $D_{4h}$ symmetry. [d] From ref 13, average values of distances symmetrically equivalent in $C_{2h}$ symmetry. [e] Atoms pairs of the first column are indicated as in Figure 1.

ticular, there is wide agreement[10,11,31] about the stable $D_{2h}$ structure of (**2**). This is also the result of our B3-LYP/cc-pVDZ calculation. In Table 1 the comparison is made with the experimental structure, assuming that the isolated molecule has $D_{2h}$ symmetry, as it is generally induced from X-ray diffraction data.[9] Going from (**1**) to (**2**) with the substitution of the methano and methine groups with isoelectronic imino groups and N atoms, respectively, the 1−21 and 6−22 distances are strongly reduced from 1.504 and 1.412 Å to 1.372 and 1.365 Å, respectively. All other distances are not so markedly changed (see Table 1). As a net result, the inner cycle 1, 21, 4, 5, 6, 22, 9, 10, 11, 23, 14, 15, 16, 24, 19, 20 has two parameters, average C−C length and largest deviation from the mean value, typical of aromatic systems and gives rise to an extended conjugation pathway in (**2**), coexisting with that already defined in (**1**).

Considering the remaining molecular systems, (**3**), (**4**), and (**5**), only (**4**) has been found in our calculation to have the stable $D_{4h}$ structure reported in Table 1. The result compares well with previous B3-LYP/6-31G** data[33] and the experimental geometry.[12] On the contrary, the calculated $D_{4h}$ structures of (**3**) and (**5**) are unstable with respect to several normal coordinates, due to the large size of the NH group and of the sulfur atom. In both cases the steric interaction is minimized displacing the molecule along the following three coordinates. The first is the out-of-plane $b_{2u}$ bending, where the four hydrogen atoms of the imino groups in (**3**) (or the four sulfur atoms in (**5**)) move alternatively up and down. The second is the doubly degenerate out-of-plane $e_g$ mode with two opposite hydrogen (sulfur) atoms oscillating in-phase and the other two fixed. The third, of $a_{2u}$ symmetry, is the counterpart of the first, i.e., the in-phase motion of all four hydrogen (sulfur) atoms out-of-plane.

The conformational changes of (**3**) and (**5**) starting from the respective $D_{4h}$ geometries are correlated in Figure 2. Displacing (**3**) along the $b_{2u}$ mode a stable structure of lower symmetry, $D_{2d}$, is optimized tilting adjacent pyrrole rings up and down with respect to the plane of the four *meso*-methine C atoms and thus giving rise to a saddle arrangement (see Figure 3, left), as usually defined for distorted porphyrins.[34−36] The equilibrium geometry is in good agreement with X-ray diffraction data on the skeleton of diprotonated 5,10,15,20-tetraphenylporphyrin $(H_4TPP)^{2+}$ and 5,10,15,20-tetramesitylporphyrin $(H_4TMP)^{2+}$.[14,16] The second stable conformer, with energy higher than $D_{2d}$ by

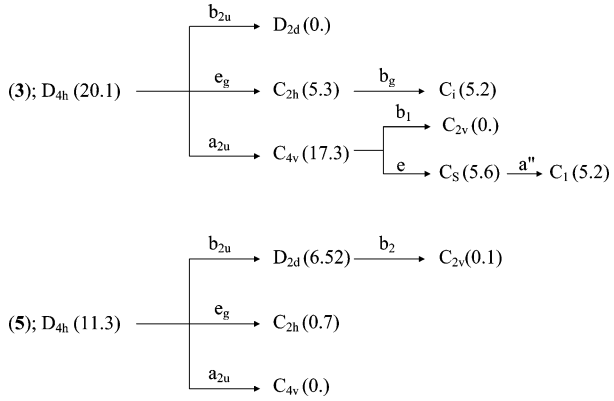


**Figure 2.** Schematic plot of the correlation between ground-state extrema of (**3**) and (**5**), top and bottom diagram, respectively. Each extremum, characterized by its symmetry and energy (with respect to the energy of the absolute minimum, kcal/mol, DF/B3-LYP/cc-pVDZ results) is related to the next ones through normal modes with imaginary frequency and symmetry species given over the arrow. The starting extremum for both (**3**) and (**5**) has $D_{4h}$ symmetry. In the top diagram the $C_{2v}$ minimum of (**3**) has a structure identical to that of the $D_{2d}$ minimum.

5.3 kcal/mol, has been obtained in two steps. Moving first the system along the $e_g$ mode a wave[34−36] $C_{2h}$ geometry is reached with $C_2$ aligned along the $C_2'$ axis of the $D_{4h}$ group and two opposite N−H bonds up and down with respect to the porphyrin mean plane. This is not a minimum structure, having one imaginary $b_g$ frequency. The final quasi-wave $C_i$ structure, 0.1 kcal/mol lower, minimizes the steric interaction between central hydrogen atoms forcing also the second pair of N−H bonds slightly outward (see Figure 3, center). These results are in close agreeement with previous findings.[17] In addition, a third conformer is found moving from $D_{4h}$ to $C_{4v}$ symmetry along the $a_{2u}$ coordinate. The dome[34−36] $C_{4v}$ geometry is itself a second-order maximum with respect to one $b_1$ and one e mode. The stable structure toward which the $C_{4v}$ geometry spontaneously shifts along the $b_1$ mode is the saddle $D_{2d}$ structure previously encountered, though now has formally only the symmetry of the $C_{2v}$ subgroup. More interesting, the other displacement of e symmetry leads to a quasi-ruffled[34−36] structure of strict $C_s$ and approximate $C_{2h}$ symmetry (with $C_2$ parallel to $C_2''$ axis of the $D_{4h}$ group, see Figure 3, right),

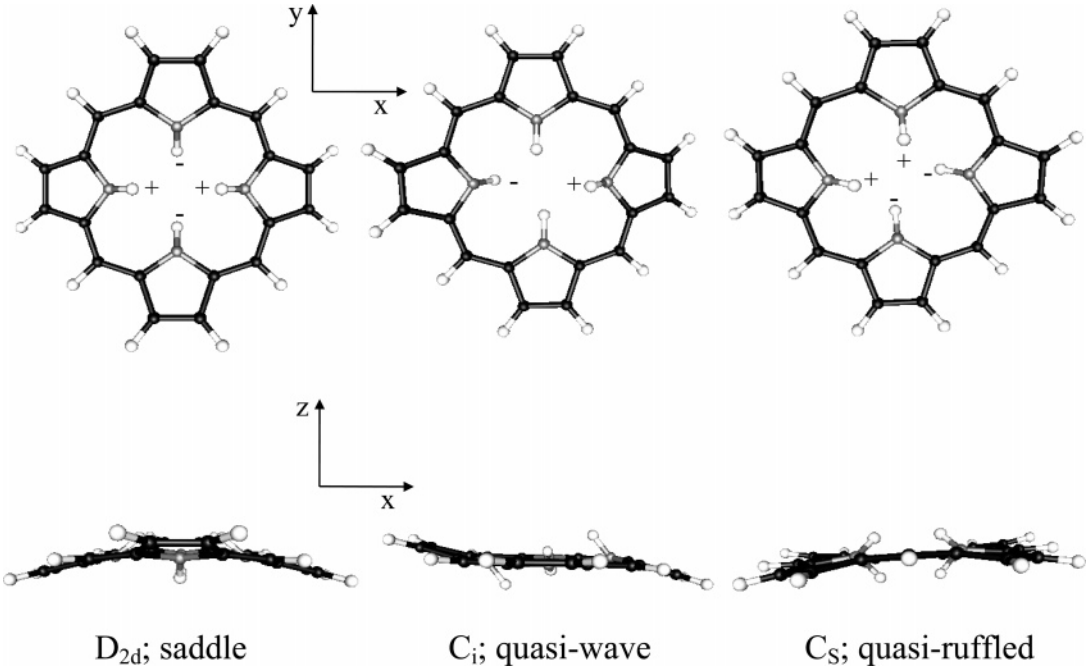


**Figure 3.** Top and side view of two stable isomers of (**3**), right $D_{2d}$ and center $C_i$, and of the saddle $C_s$, according to the calculation results and to the designations taken from ref 36. The reference system for the top and side view is indicated. Plus and minus signs indicate qualitatively the torsional arrangement of the pyrrole ring with respect to the mean porphyrin plane.

**TABLE 2: Observed[a] Core Conformations of $(H_4TMP)^{2+}$ and $(H_4TCHP)^{2+}$ and Calculated Core Conformations of (3) in $D_{2d}$ and $C_s$ Symmetry[b]**

| | $(H_4TMP)^{2+}$ | (**3**);$D_{2d}$ | $(H_4TCHP)^{2+}$ | (**3**);$C_s$ |
|---|---|---|---|---|
| $\|C_\alpha\|$ | 0.19 | 0.16 | 0.08 | 0.07 |
| $\|C_\beta\|$ | 0.67 | 0.49 | 0.16 | 0.13 |
| $\|C_m\|$ | 0.06 | 0. | 0.07 | 0.08 |
| $\|C_{20}\|$ | 0.35 | 0.26 | 0.11 | 0.10 |
| $\|N_4\|$ | 0.08 | 0.02 | 0.24 | 0.16 |
| $\|C_{20}N_4\|$ | 0.31 | 0.22 | 0.13 | 0.11 |

[a] From ref 16. [b] $|C_\alpha|$, $|C_\beta|$, $|C_m|$, $|C_{20}|$, $|N_4|$, and $|C_{20}N_4|$ are the mean absolute perpendicular displacements (Å) of the α-, β-, meso-, 20-porphyrin carbons, pyrrole nitrogens, and 24 core atoms from the 24-atoms mean plane of the porphyrin, as defined in ref 16.

characterized by one pair of adjacent pyrrole N−H's above and the other pair below the mean porphyrin plane. This is reminiscent of the diprotonated tetracyclohexa[*b*,*g*,*l*]porphyrin $(H_4TCHP)^{2+}$ structure.[15] The stable $C_1$ minimum, 0.4 kcal/mol lower than $C_s$ and almost equienergetic with the already found $C_i$ minimum, is finally reached going along the only mode, having *a″* symmetry, with imaginary frequency at the $C_s$ geometry. It has been suggested[15] that the approximate $C_{2h}$ structure is stabilized in the crystal because of the interaction of the diprotonated species with the trifluoroacetic counterion. The small energy difference between the $C_s$ (approximate $C_{2h}$) and $C_1$ conformers makes plausible this interpretation. The two stable isomers, of $D_{2d}$ (saddle) and $C_i$ (quasi-wave) symmetry, and the quasi-ruffled $C_s$ structure are sketched in Figure 3.

The calculated distortion of (**3**) in $D_{2d}$ and $C_s$ symmetry can be compared with experimental results on derivatives of the diprotonated porphyrin.[16] It has been proposed,[16] as a measure of the deviation from planarity, the set of average absolute perpendicular displacements of ring atoms (for instance, α, β, *meso* C atoms; see Table 2 for more detail), with respect to the mean porphyrin plane. The smallest distortion values have been found[16] for $(H_4TMP)^{2+}$ and 5,10,15,20-octaethylporphyrin $(H_4OEP)^{2+}$. It is reasonable to assume that these values are indicative of the intrinsic nonplanarity of the porphyrin system and affected to a minor extent by the peripheral substitution. The agreement between the calculated values of (**3**) in $D_{2d}$ symmetry with experimental data, as it is seen from Table 2, legitimates the assumption and outlines the satisfactory computational performance of the DF/B3-LYP/cc-pVDZ combination. The unusual structure of $(H_4TCHP)^{2+}$ is less distorted than that of $(H_4TMP)^{2+}$ except for $|N_4|$, the absolute average perpendicular displacement of the pyrrole N atoms with respect to the mean porphyrin plane.[15] The calculated values of the $C_s$ structure are consistent with experiment. In particular, the $|N_4|$ parameter is predicted to be the largest, as observed.[16]

According to X-ray data, (**5**) is a centrosymmetric nonplanar ring system.[13] The structure has approximate $C_{2h}$ symmetry, the $C_2$ axis being directed along the *y* axis, with reference to Figure 1. Three stable conformations of (**5**) of almost equal energy are calculated according to the diagram shown in Figure 2, bottom, distorting the molecule away from $D_{4h}$ symmetry along appropriate $e_g$, $b_{1u}$, and $a_{2u}$ modes of imaginary frequency. The dome $C_{4v}$ isomer (obtained from $D_{4h}$ with $a_{2u}$ displacement) is the absolute minimum. The wave $C_{2h}$ isomer, ≈0.7 kcal/mol above $C_{4v}$, has a structure in fair agreement with experimental data.[13] Given the circumstances, close packing of (**5**) in the crystal is probably the determining factor in favor of the $C_{2h}$ geometry. The two isomers are reported in Figure 4. There is no saddle isomer, as the $D_{2d}$ geometry has one $b_2$ imaginary frequency thus allowing the occurrence of a third isomer, of $C_{2v}$ symmetry, 0.1 kcal/mol above $C_{4v}$ and with a similar shape.

As a final consideration, we note that steric interaction between the central heteroatoms (or between the central hydrogen atoms) may qualitatively justify some structural peculiarities of the series (**3**)−(**5**). For instance, the square geometry of (**4**) can be reasonably predicted as stable on the basis of the distance between nearest oxygen neighbors in (**4**), $d_{nn} = 2.93$ Å, which is comparable to the distance of minimum contact, $2r_O = 3.04$ Å, where $r_O = 1.52$ Å is the van der Waals oxygen radius. Instead, both (**3**) and (**5**) have $D_{4h}$ structures with the former parameter, $d_{nn}$, much shorter than the latter, $2r_H$ for (**3**) and $2r_S$ for (**5**), thus generating structural instabilities. In

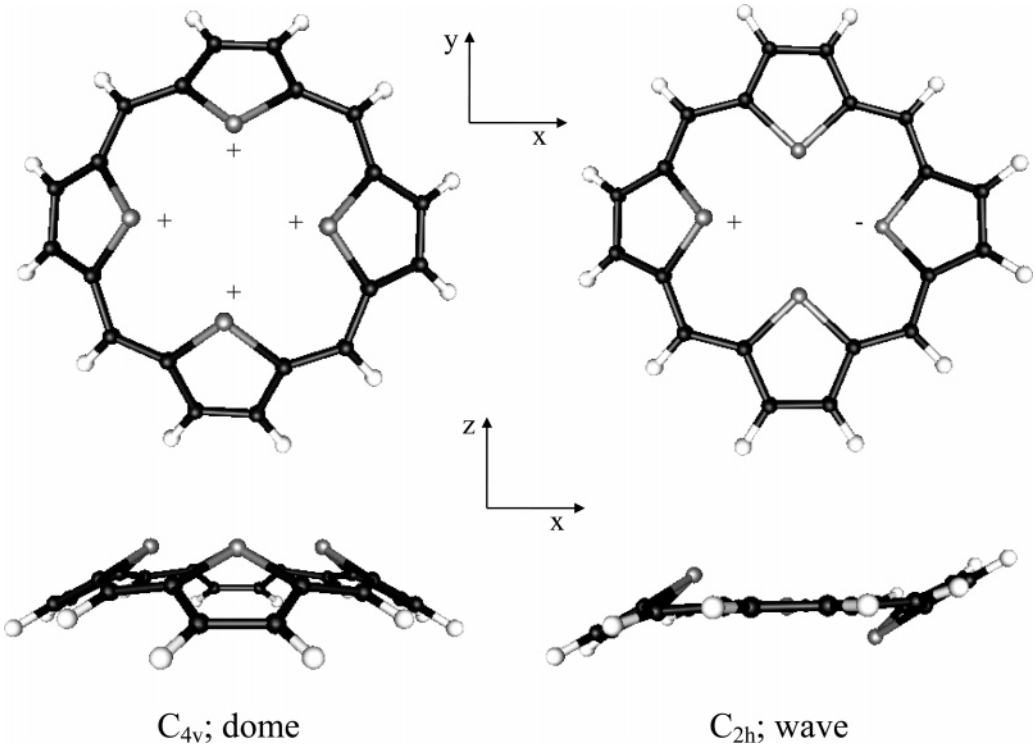


**Figure 4.** Top and side view of two stable isomers of (**5**), left $C_{4v}$ and right $C_{2h}$, according to the calculation results and to the designations taken from ref 36. The reference system for the top and side view is indicated. Plus and minus signs indicate qualitatively the torsional arrangement of the pyrrole ring with respect to the mean porphyrin plane. The third stable isomer, of $C_{2v}$ symmetry, has been omitted for the sake of simplicity, the structure being almost identical to that of the $C_{4v}$ isomer.

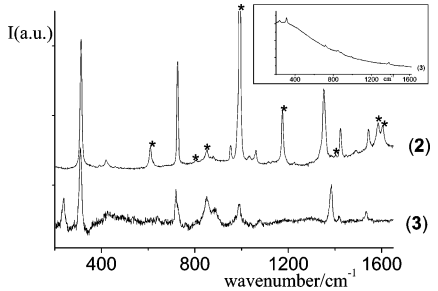


**Figure 5.** The Raman spectra of (**2**), $c = 7 \cdot 10^{-4}$ M in benzene, upper trace, and of (**3**), $c = 3 \cdot 10^{-4}$ M in HCl solution, lower trace, at room temperature exciting at 406.7 nm. The asterisks on the upper trace mark solvent bands. In the inset: experimentally observed spectrum of (**3**) (see text for details).

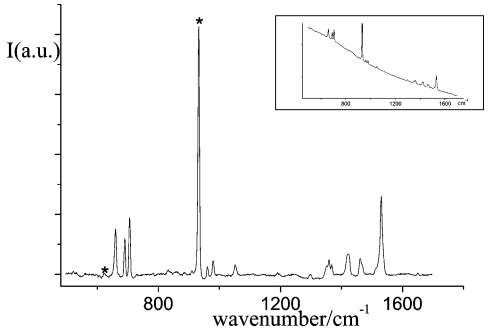


**Figure 6.** The Raman spectrum of (**4**) as a solid at room-temperature exciting at 785.0 nm. The asterisks mark Raman bands of the $ClO_4^-$ counterion. In the inset: experimentally observed spectrum of (**4**) (see text for details).

the case of (**3**) the calculation shows that only in $D_{2d}$ symmetry the steric interaction is relieved, being the nearest H···H distance 2.28 Å and the minimum contact distance 2.4 Å. So, the $D_{2d}$ conformer is expected to be energetically much lower than the others two. On the other hand, the occurrence of three almost equienergetic conformers of (**5**) correlates well with the fact that the distances between nearest neighbors are quite similar, in the range 2.91−2.96 Å, and appreciably less than twice the van der Waals radius, 3.6 Å. Thus, the three conformers are roughly hindered to the same extent, and none of them is energetically preferred over the others.

## IV. Vibrational Results

The room-temperature Raman spectra of (**3**) in HCl solution, $c = 3 \cdot 10^{-4}$ M, exciting at 406.7 nm and of (**4**) as a solid sample exciting at 785.0 nm are shown in Figures 5 and 6, respectively. For convenience, the two spectra are presented separately in the next subsections.

**A. The Near-Resonant Raman Spectrum of (3).** Due to the vicinity of the Soret band of (**3**) to the excitation wavelength,[17] the Raman spectrum is measured in near-resonance conditions. To our surprise, a diffuse emission underlies the Raman peaks, as it is seen from the inset of Figure 5. Since no signal is detected in the presence of the solvent alone, the emission has been tentatively assigned to fluorescence from the Soret band. More on this point will be reported soon. For the purpose of the present work the intrinsic Raman spectrum has been obtained subtracting the underlying emission. In the subsequent discussion weak features of the subtracted spectrum are not considered, as they may be artifacts related to the subtraction process. By comparison, the spectrum of (**2**) in benzene solution, $c = 7 \cdot 10^{-4}$ M, under identical experimental conditions is also displayed in Figure 5. No diffuse emission is observed in this case. To the best of our knowledge, though several studies deal with the Raman spectrum under different excitation conditions,[23,24,37] none has reported on (**2**) with excitation near the Soret band.

The absorption spectrum of (**3**) is dominated by the Soret band with high oscillator strength ( $f = 1.09$).[17] When excited

states, to which the transition from the ground state is strongly allowed, are close to the excitation energy, it is expected that the Raman activity is mostly induced through the Franck−Condon scattering mechanism by totally symmetric modes.[38−42] On the other hand, in the case of (**2**) the Soret band is due to a pair of quasi-degenerate states, called $B_y$ and $B_x$, of $B_{2u}$ and $B_{3u}$ symmetry species,[43] with total oscillator strength $f = 1.15$.[44,45] In near resonance with the Soret band not only $a_g$ modes but also $b_{1g}$ modes are expected to be active, due to the vibronic coupling mechanism between $B_y$ and $B_x$ for Raman intensities.[41]

Experimentally, the two spectra show a limited number (seven) of medium/strong peaks, in good correspondence each with the other, 310/312, 720/726, 990/953, 1081/1061, 1384/1352, 1418/1423, 1534/1544 $cm^{-1}$ in the order (**3**)/(**2**). Since the Raman bands of (**2**) have been assigned unambiguously to the totally symmetric species,[23,24,37] the previous point suggests that similar totally symmetric modes are active in the Raman spectrum of (**3**). In addition, four medium/weak bands of (**3**), namely 238, 643, 852, and 889 $cm^{-1}$, are observed. Finally, the spectrum of (**2**) shows three weak bands, 391, 420, and 1490 $cm^{-1}$, whose assignment is to $b_{1g}$ symmetry,[23] and a fourth, 1032 $cm^{-1}$, totally symmetric (see the next section).

**B. The Raman Spectrum of (4).** It is known[46] that (**4**) fluoresces from the lowest excited state in the spectral range 570−640 nm. Although the excitation wavelength for the Raman experiment is far from the lowest absorption of the molecule, a diffuse background fluorescence is seen even exciting (**4**) at 785.0 nm, due to the very weak absorption of the solid at this wavelength. The experimentally observed spectrum is shown in the inset of Figure 6 from which the Raman signal has been obtained removing the smoothly varying emission. Being the incident photon energy ≈0.6 eV less than the onset of the molecular $S_0 \rightarrow S_1$ absorption,[12] the spectrum is considered as predominantly due to normal Raman scattering. Modes of $a_{1g}$, $b_{1g}$, $b_{2g}$, and $e_g$ symmetry are expected to be active. Fourteen peaks (660, 690, 706, 909, 961, 979, 1051, 1189, 1298, 1359, 1368, 1422, 1461, 1530 $cm^{-1}$) of medium/strong intensity have been observed. Since the number of peaks is greater than that of the totally symmetric modes of (**4**) in $D_{4h}$ symmetry, seven (excluding C−H stretchings), it is concluded that some nontotally symmetric modes contribute comparably to $a_{1g}$ modes to the spectrum.

## V. Discussion

**A. Vibrational Calculations.** The vibrational frequencies of (**2**), (**3**), and (**4**) at the stable geometries in $D_{2h}$, $D_{2d}$, and $D_{4h}$ symmetry, respectively, have been calculated following the structural optimization and using the B3-LYP functional and the cc-pVDZ basis set. For later convenience the vibrational calculation has been performed also at the $D_{4h}$ structure of (**3**). There is a large amount of vibrational data on (**2**) from normal and resonance Raman,[23,24] infrared,[26] and fluorescence[27] spectroscopy from which the vibrational assignment has been established in great detail.[23,28] We have doubled the assignment with comparable accuracy, to our opinion, adopting a single frequency scale factor equal to 0.9816 and finding, as a result, a root-mean-square deviation from experimental values of ≈12 $cm^{-1}$. Further, we have checked that our normal mode description is essentially coincident with that already given in the reference calculation.[23,28] These results represent a good starting point for the vibrational analysis of (**3**) and (**4**).

The 114 vibrational degrees of freedom of (**3**) can be classified among the symmetry species of the $D_{2d}$ group as $\Gamma = 15a_1 + 14a_2 + 13b_1 + 16b_2 + 28e$. The same classification for the 108 vibrational modes of (**2**) in $D_{2h}$ symmetry gives $\Gamma = 19a_g + 18b_{1g} + 9b_{2g} + 8b_{3g} + 8a_u + 10b_{1u} + 18b_{2u} + 18b_{3u}$. The missing six vibrational coordinates going from (**3**) to (**2**) may be approximately described as symmetric and antisymmetric combinations of the two N−H stretchings, of the two CNH planar bendings and of the two CCN−H out-of-plane bendings. The first two coordinates belong to $a_g$ and $b_{2u}$ symmetry species, respectively, the intermediate to $b_{3u}$ and $b_{1g}$, and the final to $b_{1u}$ and $b_{3g}$ under $D_{2h}$ symmetry. Once an account is taken of this difference, it is possible to correlate the vibrational modes of (**2**) and (**3**) through the common group of higher symmetry, $D_{4h}$. A similar procedure has been reported for (**2**), dealing with the depolarization ratios of $a_g$ modes.[23] The 114 normal modes of (**3**) in $D_{4h}$ symmetry are classified as follows: $\Gamma = 10a_{1g} + 9a_{2g} + 10b_{1g} + 10b_{2g} + 9e_g + 3a_{1u} + 6a_{2u} + 5b_{1u} + 5b_{2u} + 19e_u$.

**TABLE 3: Correlation Diagrams between the $D_{2h}$ and $D_{4h}$ Point Groups and between the $D_{4h}$ and $D_{2d}$ Point Groups[a]**

| $C_2'$ $D_{2h}$ | $D_{4h}$ | $C_2'' \rightarrow C_2'$ $D_{2d}$ |
|---|---|---|
| $a_g$ | $a_{1g}$ | $a_1$ |
| $b_{1g}$ | $a_{2g}$ | $a_2$ |
| $a_g$ | $b_{1g}$ | $b_2$ |
| $b_{1g}$ | $b_{2g}$ | $b_1$ |
| $b_{2g}+b_{3g}$ | $e_g$ | e |
| $a_u$ | $a_{1u}$ | $b_1$ |
| $b_{1u}$ | $a_{2u}$ | $b_2$ |
| $a_u$ | $b_{1u}$ | $a_2$ |
| $b_{1u}$ | $b_{2u}$ | $a_1$ |
| $b_{2u}+b_{3u}$ | $e_u$ | e |

[a] The $C_2'$ axes of the $D_{4h}$ group (along $x$ and $y$ in Figure 1) are $C_2$ axes of the $D_{2h}$ group. The $C_2''$ axes of the $D_{4h}$ group (midway between $x$ and $y$ in Figure 1) are the $C_2$ axes normal to the main axis ($S_4$) of the $D_{2d}$ group.

The diagrams $D_{4h} \rightarrow D_{2h}$ and $D_{4h} \rightarrow D_{2d}$, reported in Table 3, allow the correlation between normal coordinates of (**2**) and (**3**) with similar atomic displacements. To illustrate the point let us consider a single example from Table 3. Considering the previous classifications, 10 $a_{1g}$ and 5 $b_{2u}$ modes of (**3**);$D_{4h}$ correlate with 15 $a_1$ modes of (**3**);$D_{2d}$. If the interaction terms between $a_{1g}$ and $b_{2u}$ modes due to symmetry lowering are small, there will be 10 $a_1$ modes (out of 15) having approximate $a_{1g}$ character and 5 approximate $b_{2u}$ character. On the other hand, 10 $a_{1g}$ and 10 $b_{1g}$ modes of (**3**);$D_{4h}$ correlate with only 19 $a_g$ modes of (**2**), since (**2**) has, as noted in the last paragraph, one $a_g$ mode less than the sum of $a_{1g}$ and $b_{1g}$ modes of (**3**);$D_{4h}$. In the same approximation as above 9 $a_g$ modes of (**2**) have approximate $a_{1g}$, and 10 $a_g$ modes of (**2**) have approximate $b_{1g}$ symmetry. The former 9 $a_g$ modes of (**2**) are expected to be similar to 9 $a_1$ modes of (**3**);$D_{2d}$, the tenth $a_1$ mode being the symmetric combination of the two additional N−H stretchings acquired going from (**2**) to (**3**);$D_{2d}$. Further, the remaining 5 $a_1$ modes of (**3**);$D_{2d}$ correlate with 5 $b_{1u}$ modes of (**2**), out of a total of 10 $b_{1u}$ modes, and the remaining 10 $a_g$ modes of (**2**) with 10 $b_2$ modes of (**3**);$D_{2d}$, out of a total of 16 $b_2$ modes (for both cases see Table 3).

Extending these considerations to all symmetry species and excluding for the sake of simplicity N−H and C−H stretchings from the analysis, mode correlations of nondegenerate and degenerate vibrations of (**3**);$D_{4h}$ with vibrations of (**3**);$D_{2d}$ and of (**2**) have been obtained, as shown in Tables 4 and 5. Each vibrational coordinate has been accurately considered in the three cases examining the associated atomic displacements and resorting to the Gaussian graphic option. In the same tables

**TABLE 4: Correlation between Nondegenerate Normal Frequencies of (2), (3), and (4), According to the Diagrams of Table 3, at the Stable $D_{2h}$, $D_{2d}$, and $D_{4h}$ Geometries[a]**

| (2) | (3) | | (4) | (2) | (3) | | (4) | (2) | (3) | | (4) |
|---|---|---|---|---|---|---|---|---|---|---|---|
| $D_{2h}$ | $D_{4h}$ | $D_{2d}$ | $D_{4h}$ | $D_{2h}$ | $D_{4h}$ | $D_{2d}$ | $D_{4h}$ | $D_{2h}$ | $D_{4h}$ | $D_{2d}$ | $D_{4h}$ |
| $a_g$ | $a_{1g}$ | $a_1$ | $a_{1g}$ | $b_{1g}$ | $a_{2g}$ | $a_2$ | $a_{2g}$ | $a_{1u}$ | $b_{1u}$ | $a_2$ | $b_{1u}$ |
| 303 (312) | 316 | 304 | 294 | 387 (391) | 366 | 385 | 380 | 65 | 83 | 69 | 58 |
| 720 (726) | 705 | 719 | 694 | 779 (786) | 784 | 798 | 801 | 477 | 484 | 478 | 459 |
| 956 (953) | 1001 | 994 | 931 | 970 (976) | 974 | 988 | 974 | 701 | 691 | 680 | 689 |
| 1046 (1061) | 1089 | 1087 | 1052 | 1136 (1138) | 1164 | 1172 | 1131 | 844 | 887 | 895 | 879 |
| 1363 (1352) | 1399 | 1408 | 1363 | 1220 (1226) | 1235 | 1279 | 1295 | 909 | 970 | 975 | 951 |
| 1448 (1423) | 1436 | 1443 | 1427 | 1349 (1374) | 1376 | 1391 | 1370 | | | | |
| 1569 (1544) | 1559 | 1565 | 1538 | 1390 (1388) | 1416 | 1405 | | $a_u$ | $a_{1u}$ | $b_1$ | $a_{1u}$ |
| | | | | 1607 (1600) | 1614 | 1626 | 1610 | 295 | 308 | 302 | 282 |
| $a_g$ | $b_{1g}$ | $b_2$ | $b_{1g}$ | | | | | 684 | 687 | 679 | 674 |
| 152 (155) | 138 | 148 | 137 | $b_{1g}$ | $b_{2g}$ | $b_1$ | $b_{2g}$ | 900 | 964 | 971 | 946 |
| 723 (736) | 726 | 722 | 726 | 91 (109) | 178 | 129 | 103 | | | | |
| 993 (987) | 1014 | 1011 | 962 | 411 (420) | 419 | 427 | 419 | $b_{1u}$ | $b_{2u}$ | $a_1$ | $b_{2u}$ |
| 1041 (1032) | 1084 | 1083 | 1051 | 800 (805) | 807 | 812 | 803 | 731 (731) | 1431i | 755 | |
| 1180 (1177) | 1207 | 1221 | 1197 | 1000 (1005) | 1045 | 1008 | 980 | 54 | 69 | 59 | 45 |
| 1408 (1384) | 1411 | 1404 | 1369 | 1185 (1182) | 1213 | 1220 | 1180 | 206 | 192 | 212 | 192 |
| 1514 (1490) | 1512 | 1509 | 1477 | | 1359 | 1292 | | 645 | 635 | 659 | 648 |
| 1625 (1609) | 1622 | 1641 | 1653 | 1322 (1318) | 1403 | 1405 | 1297 | 789 (785) | 834 | 849 | 829 |
| | | | | 1504 (1493) | 1617 | 1573 | 1493 | | | | |
| | | | | | | | | $b_{1u}$ | $a_{2u}$ | $b_2$ | $a_{2u}$ |
| | | | | | | | | | 179i | 448 | |
| | | | | | | | | 93 | 121 | 85 | 100 |
| | | | | | | | | 331 (335) | 364 | 327 | 322 |
| | | | | | | | | 701 (691) | 694 | 710 | 698 |
| | | | | | | | | 780 (773) | 808 | 821 | 802 |
| | | | | | | | | 862 (852) | 909 | 916 | 899 |

[a] Frequencies ($cm^{-1}$) are calculated according to the DF/B3-LYP/cc-pVDZ procedure. Under heading (**3**) − $D_{4h}$ calculated frequencies are reported for the planar square structure of (**3**). Under heading (**2**) − $D_{2h}$ experimental frequencies ($cm^{-1}$) are reported in parentheses, from refs 23, 24, 27, and 37 and our own measurements. The scale factors are 0.9816 for (**2**) and 0.9775 for (**4**), while the frequencies of (**3**) in $D_{4h}$ and $D_{2d}$ symmetry are unscaled (see text for details).

under heading (**2**) the experimental frequencies from other studies[23,24,26,37] and our own measurements are reported in parentheses. As to (**3**);$D_{2d}$ and (**3**);$D_{4h}$, the vibrational frequencies are reported as calculated ab initio, i.e., the scale factor is 1 (see next subsection). On the whole, a good correlation of normal modes is obtained going from (**2**) to (**3**);$D_{4h}$ and to (**3**);$D_{2d}$, thus justifying the previous approximation. In particular, we note that the correlation is excellent between $a_g$ modes of (**2**) and $a_1$ modes of (**3**);$D_{2d}$ forming the subset of the seven $a_{1g}$ modes of (**3**);$D_{4h}$, in agreement with the correspondence mentioned in the last section.

The 102 normal modes of (**4**) under $D_{4h}$ symmetry are divided into $9a_{1g} + 8a_{2g} + 9b_{1g} + 9b_{2g} + 8e_g + 3a_{1u} + 5a_{2u} + 5b_{1u} + 4b_{2u} + 17e_u$. Comparing with the normal mode representation of (**3**);$D_{4h}$ the following modes, $1a_{1g} + 1a_{2g} + 1b_{1g} + 1b_{2g} + 1e_g + 1a_{2u} + 1b_{2u} + 2e_u$, are missing. The difference may be easily justified noting that these modes have a simple approximate description as combinations of four N−H stretchings ($a_{1g} + b_{1g} + e_u$), four CNH bendings ($a_{2g} + b_{2g} + e_u$), and four CCN−H out-of-plane bendings ($a_{2u} + b_{2u} + e_g$). Having this point in mind, the correct correlation between normal modes of (**3**);$D_{4h}$ and (**4**) is almost straightforward, as shown in Tables 4 and 5. Note, however, that no empty entry appears in Table 4 for $a_{1g}$ and $b_{1g}$ modes of (**4**) and only one for $e_u$ modes, instead of two, in Table 5 since stretching N−H modes have been excluded from the analysis. The calculated frequency values of (**4**) have been multiplied by the scale factor 0.9775, as a result of the proposed vibrational assignment (see the third subsection).

**B. Vibrational Assignment of (3): $a_1$ Modes.** In the previous section the near-resonance Raman spectrum of (**3**) was assigned mostly to $a_1$ modes on the basis of general considerations[38−42] and of the comparison with the spectrum of (**2**) in the same experimental conditions. Here, the conclusion is supported by the results of Table 6 where the observed Raman frequencies are, within few tenths of wavenumbers, close to the $a_1$ calculated values. No $b_1$, $b_2$, or e modes satisfy this condition as closely as $a_1$ except one $b_2$ mode, 916 $cm^{-1}$ (calc), related to the 889 $cm^{-1}$ Raman peak. Since the number of experimental frequencies (12 between 200 and 1600 $cm^{-1}$) is low with respect to the number of active frequencies (61 up to 1700 $cm^{-1}$, either Raman or infrared), no attempt has been made to propose scale factors for the whole set of vibrational frequencies (74 up to 1700 $cm^{-1}$). The calculated ab initio values of (**3**);$D_{2d}$ and, for consistency, of (**3**);$D_{4h}$ are not scaled in Tables 4 and 5.

From Raman intensities it is possible to draw some inferences about the equilibrium structure of the state giving origin to the Soret band, 2E according to DF calculations.[17] Raman peaks at 310 and 1384 $cm^{-1}$ are the strongest of the spectrum, while those at 1418 and 1534 $cm^{-1}$ the weakest. The 310 $cm^{-1}$ vibration is described as uniform breathing of the inner cycle 1,21,4,5,6,22,9,10,11,23,14,15,16,24,19,20 due to $C_\alpha C_m C_\alpha$ bending and that at 1384 $cm^{-1}$ as a combined motion of $C_\alpha N$, $C_\alpha C_\beta$ stretchings and of the $C_\alpha C_m C_\alpha$ bending; in contrast, the other two vibrations are located on the outer $C_\beta C_\beta$ bonds whose stretching is accompanied by $C_\beta$-H in-plane deformations. The four vibrational coordinates are reported in Figure 7. Further, there are three $a_1$ modes, 238, 643, and 729 $cm^{-1}$, correlated to out-of-plane $b_{2u}$ vibrations of (**3**);$D_{4h}$ (see Table 4), among which the first is strongly and the other two weakly active in the Raman spectrum. The 238 $cm^{-1}$ mode is described as due to pyrrole torsions, such that the molecule becomes more planar, while the other two, 643 and 729 $cm^{-1}$, as due to $C_\beta$−H and N−H out-of-plane bendings, respectively. The three coordinates are reported in Figure 8. Since in a near-resonance Raman experiment those totally symmetric modes are enhanced which

**TABLE 5: Correlation between Degenerate Normal Frequencies of (3) and (4) and Nondegenerate Modes of (2) at the Stable $D_{2h}$, $D_{2d}$, and $D_{4h}$ Geometries, According to the Diagrams of Table 3[a]**

| (2) | (3) | | (4) | (2) | (3) | | (4) |
|---|---|---|---|---|---|---|---|
| $D_{2h}$ | $D_{4h}$ | $D_{2d}$ | $D_{4h}$ | $D_{2h}$ | $D_{4h}$ | $D_{2d}$ | $D_{4h}$ |
| $b_{2g}$; $b_{3g}$ | $e_g$ | e | $e_g$ | $b_{2u}$;$b_{3u}$ | $e_u$ | e | $e_u$ |
| 588; − | 734i | 535 | | 984(977)<br>996 | 1026 | 1001 | 975 |
| 114; 132 | 149 | 127 | 121 | | | | |
| 183; 203 | 191 | 202 | 189 | 1037(1054);<br>1035(1043) | 1080 | 1079 | 1047 |
| 424; 439 | 434 | 426 | 416 | | | | |
| 668; 669 | 662 | 665 | 660 | 1151;<br>1140(1134) | 1182 | 1180 | 1141 |
| 704; 706 | 693 | 697 | 695 | | | | |
| 778; 779 | 821 | 836 | 814 | 1229(1228);<br>1203(1177) | 1261 | 1266 | 1223 |
| 853; 854 | 899 | 905 | 890 | | | | |
| 904; 907 | 968 | 973 | 949 | 1250;<br>1284 | 1296 | 1305 | 1311 |
| $b_{2u}$; $b_{3u}$ | $e_u$ | e | $e_u$ | 1359(1357);<br>− | 1374 | 1376 | 1365 |
| 284;<br>309(310) | 319 | 297 | 284 | | | | |
| | | | | 1417(1406);<br>1410(1396) | 1418 | 1416 | |
| 351(357);<br>351 | 353 | 360 | 355 | | | | |
| | | | | 1503(1490);<br>1532(1561) | 1501 | 1493 | 1449 |
| 742(745);<br>725(723) | 738 | 739 | 732 | | | | |
| | | | | 1558(1540);<br>1526 | 1523 | 1531 | 1499 |
| 775;<br>778(780) | 779 | 793 | 789 | | | | |
| | | | | 1612;<br>1414(1412) | 1591 | 1595 | 1573 |
| 954(951);<br>975(971) | 987 | 984 | 934 | | | | |

[a] Frequencies ($cm^{-1}$) are calculated according to the DF/B3-LYP/cc-pVDZ procedure. Under heading (**3**) − $D_{4h}$ calculated frequencies are reported for the planar square structure of (**3**). Under heading (**2**) − $D_{2h}$ experimental frequencies ($cm^{-1}$) are reported in parentheses, from refs 23, 24, 27, and 37. The scale factors are 0.9816 for (**2**) and 0.9775 for (**4**), while the frequencies of (**3**) in $D_{4h}$ and $D_{2d}$ symmetry are unscaled (see text for details).

**TABLE 6: On the Left—Vibrational Assignment of the Raman Spectrum of (3), $\lambda_{exc}$ = 406.7 nm, Acid Solution, Room Temperature[a] and on the Right—Vibrational Assignment of the Raman ($\lambda_{exc}$ = 785 nm; Crystal Grain) and of the Infrared (Nujol Mull) Spectrum of (4)[b]**

| (3) Raman | | (4) Raman | | |
|---|---|---|---|---|
| exp | calc | exp | calc | $I_R$ |
| 238 m | 212 ($a_1$) | | | |
| 310 s | 304 ($a_1$) | | | |
| 643 w | 659 ($a_1$) | | | |
| | | 660 ms | 659 ($e_g$) | ≈0. |
| | | 689 ms | 695 ($e_g$) | 0.02 |
| 720 m | 719 ($a_1$) | 706 ms | 694 ($a_{1g}$) | 0.14 |
| 729 sh | 755 ($a_1$) | | | |
| 852 m | 849 ($a_1$) | | | |
| 889 mw | 916 ($b_2$) | | | |
| 990 mw | 994 ($a_1$) | 909 w | 930 ($a_{1g}$) | 0.40 |
| | | 961 mw | 962 ($b_{1g}$) | 0.18 |
| | | 979 mw | 980 ($b_{2g}$) | 0.02 |
| 1081 w | 1087 ($a_1$) | 1051 mw | 1052 ($a_{1g}$) | 0.05 |
| | | 1190 vw | 1180 ($b_{2g}$) | 0.003 |
| | | 1297 w | 1296 ($b_{2g}$) | 0.28 |
| 1384 s | 1408 ($a_1$) | 1360 mw | 1362 ($a_{1g}$) | 0.24 |
| | | 1368 mw | 1369 ($b_{1g}$) | 0.31 |
| 1418 w | 1443 ($a_1$) | 1422 mw | 1427 ($a_{1g}$) | 0.56 |
| | | 1461 mw | 1477 ($b_{1g}$) | 0.74 |
| | | 1468 sh | 1493 ($b_{2g}$) | 0.01 |
| 1534 w | 1565 ($a_1$) | 1530 s | 1538 ($a_{1g}$) | 1. |
| | | 1646 vw | 1652 ($b_{1g}$) | 0.02 |
| | | infrared | | |
| | | 696 w | 698 ($a_{2u}$) | 0.06 |
| | | 739 w | 732 ($e_u$) | 0.06 |
| | | 798 m | 789 ($e_u$) | 0.05 |
| | | 819 m | 802 ($a_{2u}$) | 0.40 |
| | | 900 s | 899 ($a_{2u}$) | 1. |
| | | 936 s | 934 ($e_u$) | 1.40 |
| | | 972 w | 975 ($e_u$) | 0.08 |
| | | 1049 s | 1047 ($e_u$) | 0.30 |
| | | 1149 m | 1141 ($e_u$) | 0.26 |
| | | 1221 vw | 1223 ($e_u$) | 0.14 |
| | | 1446 s | 1449 ($e_u$) | 0.84 |
| | | 1495 m | 1499 ($e_u$) | 0.52 |
| | | 1569 mw | 1573 ($e_u$) | 0.22 |

[a] The calculated frequencies ($cm^{-1}$) are unscaled; the experimental band intensities are denoted as strong (s), medium (m), weak (w), and as their combinations; the symmetry species, in parentheses, are relative to $D_{2d}$ symmetry. [b] The calculated frequencies ($cm^{-1}$) are scaled by the factor 0.9775; the experimental band intensities are denoted as before; the symmetry species, in parentheses, are relative to $D_{4h}$ symmetry. Calculated Raman ($I_R$) intensities are relative to that of the 1538 $cm^{-1}$ ($a_{1g}$) mode, while calculated infrared intensities ($I_{IR}$) are relative to that of the 899 $cm^{-1}$ ($a_{2u}$) mode.

favor the structural change from the ground to the excited state,[41] the qualitative indication coming from our intensity data is that the equilibrium geometry of the 2E state is characterized by the expansion and the enhanced planarity of the inner cycle with respect to the ground state.

**C. Vibrational Assignment of (4).** *1. The Raman Spectrum.* The vibrational assignment of the Raman frequencies is summarized in Table 6. A good agreement between calculated and observed values is obtained using the scale factor 0.9775, derived from Raman and infrared data. The correlation between vibrational modes of (**3**) and (**4**) is also shown in the same table. An interesting point concerning Raman intensities of correlated modes emerges from our assignment. Due to the different excitation conditions, the intensities of similar totally symmetric modes change markedly. For instance, the strong Raman peak of (**3**) at 1384 $cm^{-1}$ has a medium/weak counterpart in (**4**) at 1360 $cm^{-1}$. On the contrary, the weak 1534 $cm^{-1}$ band of (**3**) is correlated with the strongest band of (**4**), 1530 $cm^{-1}$. Since Raman intensities calculated by the Gaussian program are "normal", i.e., for excitation conditions far from electronic resonances, they can be reasonably compared only with the Raman data on (**4**). The largest intensity is predicted for the 1530 $cm^{-1}$ band, as observed. The calculated intensity of all the other bands is generally in fair agreement with observed intensities.

*2. The Infrared Spectrum.* Our calculation results have been compared with the infrared spectrum of (**4**) in a Nujol mull at room temperature, taken from the master degree of Dr. Knipp and kindly provided to us by Prof. G. Hohlneicher (University of Köln, Germany). The spectrum, shown in Figure 9 in the range 400−1700 $cm^{-1}$, is discussed recalling that the only modes of (**4**) infrared active belong to $a_{2u}$ and $e_u$ symmetry. First of all, some of the observed bands are due to the counterion, $ClO_4^-$, and to the Nujol mull. The two infrared active vibrations of $ClO_4^-$, $\omega_3$ and $\omega_4$, occurring in the free ion[47] at 1128 and 645 $cm^{-1}$, extend in the range 1096−1145 and 626−635 $cm^{-1}$ in perchlorate crystals.[48,49] The two strongest bands of the infrared spectrum, centered at 1096 and 623 $cm^{-1}$,

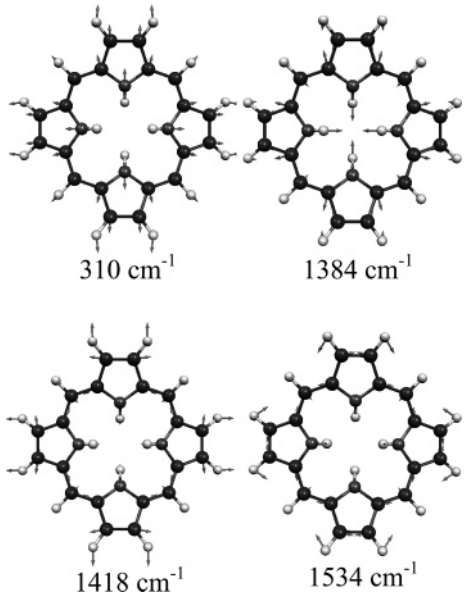


**Figure 7.** Totally symmetric, approximately in-plane, vibrations of (**3**);$D_{2d}$: atomic displacements of four normal modes, two strongly active (top, 310 and 1384 $cm^{-1}$) and two weakly active (bottom, 1418 and 1534 $cm^{-1}$) in the Raman spectrum exciting at 406.7 nm. Shaded spheres are carbon (large size) and hydrogen (small size) atoms; black spheres are nitrogen atoms.

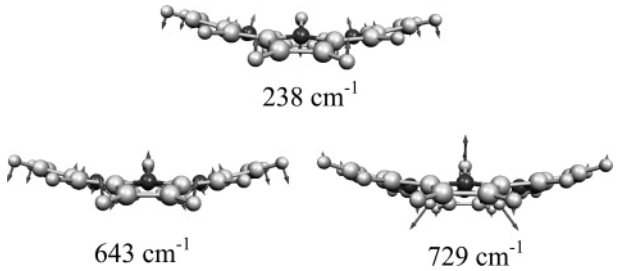


**Figure 8.** Totally symmetric, approximately out-of-plane, vibrations of (**3**);$D_{2d}$: atomic displacements of three normal modes, one active (top, 238 $cm^{-1}$) and two weakly active (bottom, 643 and 729 $cm^{-1}$) in the Raman spectrum exciting at 406.7 nm. Shaded spheres are carbon (large size) and hydrogen (small size) atoms; black spheres are nitrogen atoms.

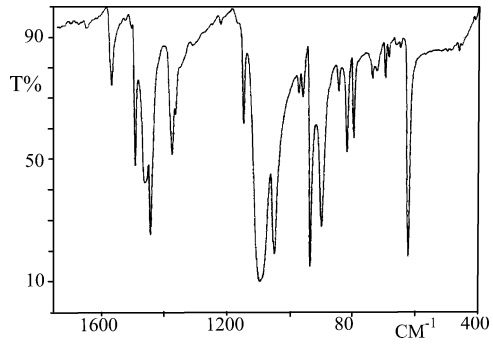


**Figure 9.** The infrared spectrum of (**4**) in a Nujol mull at room temperature in the 400−1700 $cm^{-1}$ spectral range (further details in the text).

are attributed to $ClO_4^-$. In addition, comparing our own infrared spectrum of the pure mull with that of Figure 9, Nujol bands at 1461, 1378, 1354 (sh), 1305, and 720 $cm^{-1}$ have been identified in the spectrum.

Of the expected five modes of $a_{2u}$ symmetry, only three occur above 400 $cm^{-1}$, at 696, 819, and 900 $cm^{-1}$ (see Table 6). These are out-of-plane C−H bendings among which the third, the out-of-plane in-phase $C_m$−H bending, is associated with one of the strongest bands on experimental and computational grounds. The $a_{2u}$ modes correlate with equally intense $b_{1u}$ modes of (**2**),[25] observed at 691, 773, and 852 $cm^{-1}$. There are twelve $e_u$ modes above 400 $cm^{-1}$ (excluding C−H stretchings), 10 of which are observed at 739, 798, 936, 972, 1049, 1149, 1221, 1446, 1495, and 1569 $cm^{-1}$. The two remaining, with almost vanishing calculated intensity, are expected between 1340 and 1400 $cm^{-1}$ and much probably buried under the strong 1365 $cm^{-1}$ Nujol band. Combining the infrared and Raman assignments, an average scale factor 0.9775 and a root-mean-square deviation of calculated from experimental frequency values equal to 8.6 $cm^{-1}$ have been determined.

## VI. Conclusions

In this paper structural and vibrational properties of tetraoxaporphyrin dication and of isoelectronic diprotonated porphyrin have been investigated. Structural calculations have been performed also on tetrathiaphorphyrin and on the carbon analogue of porphyrin. While for (**4**) the $D_{4h}$ structure is predicted to be stable, (**3**) and (**5**) deviate from planarity, due to the steric interaction between central atoms. As a result several stable conformations have been found for (**3**) and (**5**). In addition to the known $D_{2d}$ and $C_i$ conformers, (**3**) has in particular a third conformer of approximate $C_{2h}$ symmetry, in good agreement with the ruffled geometry of diprotonated tetracyclohexa[*b*,*g*,*l*]porphyrin.

The vibrational dynamics of (**3**) and (**4**) has been considered in the second part of this work. The Raman spectra of (**3**) and (**4**) have been measured in different excitation conditions, i.e., in near-resonance conditions with the Soret band, the first, and far from electronic resonances, the second. The mode correlation between (**2**), (**3**), and (**4**) has been the basis of the vibrational assignment for the latter two systems. On the whole, this study indicates, as in previous cases,[18,19] that DF calculations with high quality basis sets may be reliably applied to molecular systems of medium/large size and give substantial help for an accurate analysis of the vibrational spectra.

**Acknowledgment.** The authors are greatly indebted to Prof. E. Vogel (University of Köln, Germany) for kindly providing the perchlorate salt of tetraoxaporphyrin and for critical reading of the manuscript. The authors also thank Prof. G. Hohlneicher (University of Köln, Germany) for permission to use the infrared spectrum of (**4**). One of us (I.J.) thanks the Italian Ministero degli Affari Esteri and Croatian Ministry of Science, Education and Sport for a grant under Italian, Croatian cooperation.

## References and Notes

(1) *The Porphyrins*; Dolphin, D., Ed.; Academic Press: New York, 1978; Vol. I−VII.

(2) Battersby, A. R.; Fookes, C. J. R.; Matcham, G. W. J.; McDonald, E. *Nature (London)* **1980**, *285*, 17−21.

(3) Chandrashekar, T. K.; Venkatraman, S. *Acc. Chem. Res.* **2003**, *36*, 676−691.

(4) Chou, J. H.; Nalwa, H. S.; Kosal, M. E.; Rakow, N. A.; Suslick, K. S. In *Porphyrin Handbook*; Kadish, K. M., Smith, K. M., Guilard, R., Eds.; Academic Press: San Diego, 1999; Vol. VI, Chapter 41.

(5) Pandey, R. K.; Zheng, R. K. In *Porphyrin Handbook*; Kadish, K. M., Smith, K. M., Guilard, R., Eds.; Academic Press: San Diego, 1999; Vol. VI, Chapter 43.

(6) Gouterman, M. In *The Porphyrins*; Dolphin, D., Ed.; Academic Press: New York, 1978; Vol. III, p 1−165.

(7) Vogel, E.; Balci, M.; Pramod, K.; Koch, P.; Lex, J.; Ermer, O. *Angew. Chem. Int. Ed. Engl.* **1987**, *26*, 928−931.

(8) Waluk, J.; Muller, M.; Swiderek, P.; Kocher, M.; Vogel, E.; Hohlneicher, G.; Michl, J. *J. Am. Chem. Soc.* **1991**, *113*, 5511−5527.

(9) Chen, B. M. L.; Tulinski, A. J. *J. Am. Chem. Soc.* **1972**, *94*, 4144−4151.

(10) Almlof, J.; Fischer, T. H.; Gassman, P. G.; Ghosh, A.; Haser, M. *J. Phys. Chem.* **1993**, *97*, 10964−10970.
(11) Kozlowski, P. M.; Zgierski, M. Z.; Pulay, P. *Chem. Phys. Lett.* **1995**, *247*, 379−385.
(12) Vogel, E.; Haas, W.; Knipp, B.; Lex, J.; Schmickler, H. *Angew. Chem., Int. Ed. Engl.* **1988**, *27*, 406−409.
(13) Vogel, E.; Rohrig, P.; Sicken, M.; Knipp, B.; Herrmann, A.; Pohl, M.; Schmickler, H.; Lex, J. *Angew. Chem., Int. Ed. Engl.* **1989**, *28*, 1651−1655.
(14) Stone, A.; Fleischer, E. B. *J. Am. Chem. Soc.* **1968**, *90*, 2735−2747.
(15) Senge, M. O.; Forsyth, T. P.; Nguyen, L. T.; Smith, K. M. *Angew. Chem., Int. Ed. Engl.* **1994**, *33*, 2485−2487.
(16) Cheng, B.; Munro, O. Q.; Marques, H. M.; Scheidt, W. R. *J. Am. Chem. Soc.* **1997**, *119*, 10732−10742.
(17) Chen, D.-M.; Liu, X.; He, T.-J.; Liu, F.-C. *Chem. Phys.* **2003**, *289*, 397−407.
(18) Gellini, C.; Salvi, P. R.; Vogel, E. *J. Phys. Chem.* **2000**, *104*, 3110−3116.
(19) Moroni, L.; Gellini, C.; Salvi, P. R.; Liu, C.-J.; Vogel, E. *J. Phys. Chem. A* **2002**, *106*, 6554−6562.
(20) Martin, J. M. L.; El-Yazal, J.; Francois, J.-P. *J. Phys. Chem.* **1996**, *100*, 15358−15367.
(21) Langhoff, S. R. *J. Phys. Chem.* **1996**, *100*, 2819−2841.
(22) Cane', E.; Miani, A.; Palmieri, P.; Tarroni, R.; Trombetti, A. *J. Chem. Phys.* **1997**, *106*, 9004−9012.
(23) Kozlowski, P. M.; Jarzecki, A. A.; Pulay, P.; Li, X.-Y.; Zgierski, M. Z. *J. Phys. Chem.* **1996**, *100*, 13985−13992.
(24) Plus, R.; Lutz, M. *Spectrosc. Lett.* **1974**, *7*, 73−84.
(25) Radziszewski, J. G.; Nepras, M.; Balaji, V.; Waluk, J.; Vogel, E.; Michl, J. *J. Phys. Chem.* **1995**, *99*, 14254−14260.
(26) Radziszewski, J. G.; Nepras, M.; Balaji, V.; Waluk, J.; Vogel, E.; Michl, J. *J. Am. Chem. Soc.* **1991**, *113*, 5511−5527.
(27) Radziszewski, J. G.; Waluk, J.; Nepras, M.; Michl, J. *J. Phys. Chem.* **1991**, *95*, 1963−1969.
(28) Kozlowski, P. M.; Jarzecki, A. A.; Pulay, P. *J. Phys. Chem.* **1996**, *100*, 13985−13992.
(29) Frisch, M. J.; Trucks, G. W.; Schlegel, H. B.; Scuseria, G. E.; Gill, P. M. W.; Stratmann, R. E.; Burant, J. C.; Dapprich, S.; Millam, J. M.; Daniels, A. D.; Kudin, K. N.; Strain, M. C.; Farkas, O.; Tomasi, J.; Barone, V.; Cossi, M.; Cammi, R.; Mennucci, B.; Pomelli, C.; Adamo, C.; Clifford, S.; Ochterski, J.; Johnson, B. G.; Robb, M. A.; Cheeseman, J. R.; Keith, T.; Petersson, G. A.; Montgomery, J. A.; Raghavachari, K.; Al-Laham, M. A.; Zakrzewski, V. G.; Ortiz, J. V.; Foresman, J. B.; Cioslowski, J.; Stefanov, B. B.; Liu, G.; Liashenko, A.; Piskorz, P.; Komaromi, I.; Cui, Q.; Morokuma, K.; Nanayakkara, A.; Challacombe, M.; Malik, D. K.; Rabuk, A. D.; Peng, C. Y.; Ayala, P. Y.; Chen, W.; Wong, M. W.; Andres, J. L.; Replogle, E. S.; Gomperts, R.; Martin, R. L.; Fox, D. J.; Binkley, J. S.; Defrees, D. J.; Baker, J.; Stewart, J. P.; Head-Gordon, M.; Gonzalez, C.; Pople, J. A. *Gaussian 98, revision A.9*; Gaussian Inc.: Pittsburgh, PA, 1998.
(30) Ghosh, A.; Almlof, J. *J. Phys. Chem.* **1995**, *99*, 1073−1075.
(31) Merchan, M.; Orti, E.; Roos, B. O. *Chem. Phys. Lett.* **1994**, *221*, 136−144.
(32) Reimers, J. R.; Lu, T. X.; Crossley, M. J.; Hush, N. S. *J. Am. Chem. Soc.* **1995**, *117*, 2855−2861.
(33) Malsh, K.; Roeb, M.; Karuth, V.; Hohlneicher, G. *Chem. Phys.* **1998**, *227*, 331−348.
(34) Ravikanth, M.; Chandrashekar, T. K. *Struct. Bonding* **1995**, *82*, 105−188.
(35) Jentzen, W.; Simpson, M. C.; Hobbs, J. D.; Song, X.; Ema, T.; Nelson, N. Y.; Medforth, C. J.; Smith, K. M.; Veyrat, M.; Mazzanti, M.; Ramasseul, R.; Marchon, J.-C.; Takeuchi, T.; Goddard, W. A., III; Shelnutt, J. A. *J. Am. Chem. Soc.* **1995**, *117*, 11085−11097.
(36) Nurco, D. J.; Medforth, C. J.; Forsyth, T. P.; Olmstead, M. M.; Smith, K. M. *J. Am. Chem. Soc.* **1996**, *118*, 10918−10919.
(37) Solovyov, K. N.; Gladkov, L.; Gradyushko, A. T.; Ksenofontova, N. M.; Shulga, A. M.; Starukhin, A. S. *J. Mol. Struct.* **1978**, *45*, 267−305.
(38) Albrecht, A. C. *J. Chem. Phys.* **1961**, *34*, 1476−1484.
(39) Albrecht, A. C.; Hutley, M. C. *J. Chem. Phys.* **1971**, *55*, 4438−4443.
(40) Tang, J.; Albrecht, A. C. In *Raman Spectroscopy, Theory and Practice*; Szymansky, H. A., Ed.; Plenum: New York, 1970.
(41) Clark, R. J. H.; Dines, T. J. *Angew. Chem., Int. Ed. Engl.* **1986**, *25*, 131−158.
(42) Siebrand, W. M.; Zgierski, M. Z. In *Excited states*; Lim, E. C., Ed.; Academic Press: New York, 1979; Vol. 4, pp 1−135.
(43) Serrano-Andres, L.; Merchan, M.; Rubio, M.; Roos, B. O. *Chem. Phys. Lett.* **1998**, *295*, 195−203.
(44) Edwards, L.; Dolphin, D. H.; Gouterman, M.; Adler, A. D. *J. Mol. Spectry* **1986**, *38*, 16−32.
(45) Nagashima, U.; Takada, T.; Ohno, K. *J. Chem. Phys.* **1986**, *85*, 4524−4529.
(46) Bachmann, A.; Gerson, F.; Gescheidt, G.; Vogel, E. *J. Am. Chem. Soc.* **1992**, *114*, 10855−10860.
(47) Ross, S. D. *Inorganic Infrared and Raman Spectra*; McGraw-Hill: London, 1972.
(48) Bini, R.; Foggi, P.; Salvi, P. R.; Schettino, V. *J. Phys. Chem.* **1990**, *94*, 6653−6658.
(49) Kloprogge, J. T.; Wharton, D.; Hickey, L.; Frost, R. L. *Am. Mineral.* **2002**, *87*, 623−629.